Naftali (Tuli) Herscovici
AnTeg
52 Agnes Drive
Framingham, MA 01901 USA
Tel: +1 (508) 788-5152
Fax: +1 (508) 788-6226
E-mail: tuli@ieee.org

Christos Christodoulou
Department of Electrical and
Computer Engineering
University of New Mexico
Albuquerque, NM 87131-1356 USA
Tel: +1 (505) 277-6580
Fax: +1 (505) 277-1439
E-mail: christos@eece.unm.edu

Uniform Circular Arrays for Smart Antennas

Panayiotis Ioannides and Constantine A. Balanis

Department of Electrical Engineering, Arizona State University
Tempe, AZ 85287-5706
E-mail: balanis@asu.edu

Abstract

As the growing demand for mobile communications constantly increases, the need for better coverage, improved capacity, and higher transmission quality rises. Thus, a more efficient use of the radio spectrum is required. *Smart antenna systems* are capable of efficiently utilizing the radio spectrum and, thus, hold a promise for an effective solution to the present wireless systems' problems, while also achieving reliable and robust high-speed high-data-rate transmission. Although numerous studies for smart antennas have already been conducted using rectilinear arrays, including mostly *uniform linear arrays* (ULAs) and *uniform rectangular arrays* (URAs), not as much effort has been devoted to other configurations. In this paper, the performance of smart antennas with *uniform circular arrays* (UCAs) is examined. A profound justification for this selection is the symmetry possessed by uniform circular arrays. This property provides uniform circular arrays with a major advantage: the ability to scan a beam azimuthally through 360° with little change in either the beamwidth or the sidelobe level. With the use of uniform circular arrays, the two main issues related to smart antennas – estimation of the direction of arrival from incoming signals and beamforming – are both examined.

Keywords: Antenna arrays; adaptive arrays; circular arrays; land mobile radio cellular systems; smart antennas; MUSIC; ESPRIT; direction of arrival estimation; array signal processing

1. Introduction

Smart antennas, or adaptive arrays, have gained great interest among researchers during recent years. Wireless operators are currently searching for new technologies that would be implemented into the existing wireless communications infrastructures to provide broader bandwidth per user channel, better quality, and new value-added services [1]. Such research efforts will enable wireless carriers to maximize the spectral efficiency of their networks so as to meet the explosive growth of the wireless communications industry, and so as to take advantage of the huge market opportunity [2].

Deployed at the base station of the existing wireless infrastructure, smart antennas are capable of bringing outstanding capacity improvement (very important in urban and densely populated areas) to the frequency-resource-limited radio-communications system by an efficient frequency-reuse scheme [1]. This unique feature has been made feasible through the impressive advances in the field of digital signal processing, which enable smart antennas to dynamically tune out interference while focusing on the intended user [3, 4].

With the direction-finding ability of smart antennas, new value-added services, such as *position location* (PL) services for an emergency call, fraud detection, intelligent transportation systems,

law enforcement, accident reporting, etc., are also becoming reality [4-6]. Smart antennas are also deployed in ad hoc networks or wireless local-area networks (WLANs), for example, with mobile terminals (notebooks, PDAs, etc.) in a wireless network. The direction-finding ability supports the design of the packet-routing protocol, which decides the manner in which packets are relayed. The beamforming or interference-suppression ability makes it possible to increase the *throughput* at the network nodes, which is limited by interference from neighboring nodes [7, 8].

Until now, the investigation of smart antennas suitable for wireless communication systems has involved primarily rectilinear arrays: *uniform linear arrays* (ULAs) and *uniform rectangular arrays* (URAs). Different algorithms have been proposed for the estimation of the *directions of arrival* (DOAs) of signals arriving at the array, and several adaptive techniques have been examined for the shaping of the radiation pattern under different constraints imposed by the wireless environment. Furthermore, in the literature for adaptive antennas, so far little attention has been paid to circular array topologies, despite their ability to offer a number of advantages. An obvious advantage results from the symmetry of the uniform circular array structure. Due to the fact that a uniform circular array does not have edge elements, directional patterns synthesized with a uniform circular array can be electronically rotated in the plane of the array without significant change in the beam shape.

A key component of smart antenna technology is *adaptive beamforming*, which simultaneously places an antenna radiation pattern beam maximum towards the intended user or *signal of interest* (SOI), and ideally places nulls toward directions of interfering signals or *signals not of interest* (SNOIs). In this letter, we investigate adaptive beamforming with uniform circular arrays. In addition, we compare the beamforming performance of uniform circular and uniform rectangular arrays.

In this paper, we investigate uniform circular arrays for smart-antenna purposes. Two key components of smart-antenna technology examined here are *direction-of-arrival* (DOA) estimation and *adaptive beamforming*. With the former, and the aid of a signal processor, it is feasible to determine the angles from which sources transmit signals towards an antenna array. With the latter, an antenna radiation pattern beam maximum can be simultaneously placed towards the intended user or *signal of interest* (SOI), and, ideally nulls can be placed towards directions of interfering signals or *signals not of interest* (SNOIs). We consider two different approaches for DOA estimation, the MUSIC and the ESPRIT algorithms. For beamforming with uniform circular arrays, we examine both the one-dimensional and two-dimensional cases. For the one-dimensional case, beamforming is performed either along a conical cut for a fixed elevation, or along an elevation for a fixed azimuth. Furthermore, for each beamforming example, the corresponding amplitude and phase excitations of each antenna element of the uniform circular array are provided.

2. Narrowband Beamforming with a Uniform Linear Array

Pattern-synthesis methods with uniform linear arrays have been extensively studied in the context of adaptive beamforming. Whereas the uniform linear array is the simplest array geometry that allows array-processing techniques to be easily applied, it possesses some drawbacks, which lead to the necessity of studying other geometries, as well. Because uniform linear arrays utilize edge elements, all azimuths are not treated equally, and their field-of-view is limited.

To demonstrate this deficiency, and referring to Figure 1, we assume that a uniform linear array is employed at the *base station* (BS) of a wireless communication system for narrowband beamforming applications. During reception, the weighted signals are summed together, producing an output signal that is expressed as [9, 10]

$$y(t,\theta)=\sum_{n=0}^{N-1} w_n x\left(t-n\frac{d}{c}\sin\theta\right), \tag{1}$$

where $x(t)$ is the signal received at the first element, d is the distance between adjacent elements, c is the free-space propagation speed (the speed of light), and θ is the angle of arrival. In the frequency domain, Equation (1) can be written as follows:

$$Y(f,\theta)=\sum_{n=0}^{N-1} w_n X(f) e^{-j2\pi fn\frac{d}{c}\sin\theta}, \tag{2}$$

or

$$H(f,\theta)\triangleq\frac{Y(f,\theta)}{X(f)}=\sum_{n=0}^{N-1} w_n e^{-j2\pi fn\frac{d}{c}\sin\theta}. \tag{3}$$

For narrowband beamforming, f is constant and θ is variable. For the beam to be directed towards the desired direction, θ, the weighting coefficient, w_n, must be set equal to [10]

$$w_n=e^{j2\pi fn\frac{d}{c}\sin\theta_0},\quad n=0,1,\ldots,N-1. \tag{4}$$

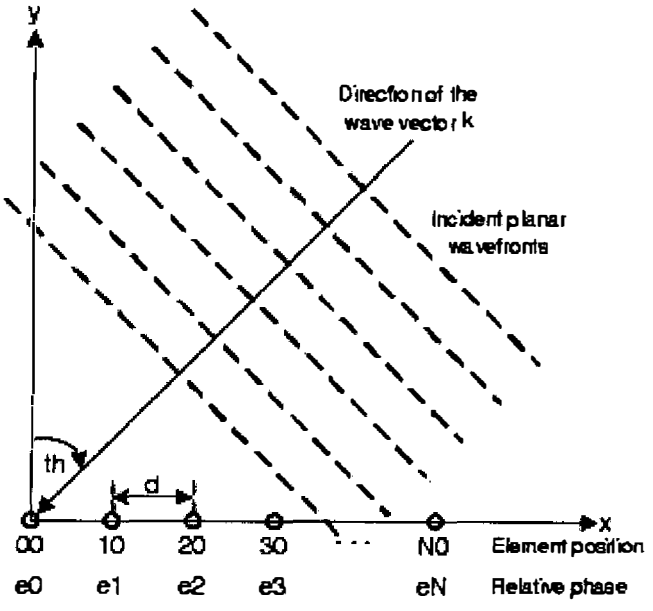

Figure 1. The array response vector for a uniform linear array [11].

In other words, for $\theta = \theta_0$, Equation (3) reduces to

$$H(f,\theta_0) = N, \tag{5}$$

which is the maximum attainable amplitude obtained by beamforming for complex weights of the same magnitude.

Figure 2a shows the normalized $|H(f,\theta)|$ for a uniform linear array with $N = 8$, $d = c/2f = \lambda/2$, and $\theta_0 = 60°$. As can be seen, a symmetrical pattern appears about the antenna axis ($\theta = \pm 90°$), since $\sin(90° - \theta) = \sin(90° + \theta)$ and $\sin(-90° - \theta) = \sin(-90° + \theta)$. This produces one more undesired main beam towards $\theta = 120°$. This is a major drawback in smart-antenna applications since it causes front-back ambiguity. The use of directive elements can eliminate the additional undesired main beam. Typically, the azimuthal field of a uniform linear array must be restricted to a half plane ($\theta \le 180°$). However, in practice the field of view of a uniform linear array is restricted to 120°. To justify this bound, we consider another example of a uniform linear array with $N = 10$, $d = \lambda/2$, and $\theta_0 = 45°$. As shown in the resulting beam pattern of Figure 2b, there is a loss of spatial resolution near the end-fire directions since the sharpness of the beams reduces considerably for $|\theta_0| > 60°$. (Spatial resolution influences the performance of an antenna array. For instance, lower resolution leads to lower directivity of the main beam in beamforming applications, and a reduced ability to separate between two closely spaced signals in direction-of-arrival estimation [12].) For this reason, the angular range of operation for a uniform linear array is restricted to $|\theta_0| \le 60°$ and, therefore, the total angle of coverage is not more than 120°. Moreover, with uniform linear arrays, the beams formed as the array is steered away from boresight broaden significantly [13].

A short-term solution to providing full azimuthal coverage is to use several uniform linear arrays, arranged in a triangular or rectangular shape, as shown in Figure 3, or to rotate the uniform linear array a few times in order to cover the full azimuthal spread [14]. However, the drawback of the former solution is the requirement of using several uniform linear arrays, and hence increasing the cost, as well the collection and processing of additional data.

In general, uniform linear arrays do not provide an appropriate solution to scenarios wherein 360° fields of view are required. In terms of radio propagation, especially in a multipath-rich environment, the signals arrive at the mobile terminal potentially from any azimuthal angle. In these scenarios – which are common in surveillance, cellular phones, etc. – the natural choice is a *uniform circular array* (UCA) [14]. Beyond entire azimuthal coverage, uniform circular arrays can provide a certain degree of source-elevation information (depending on the array's element beam pattern). Note that a uniform rectangular array with non-omnidirectional elements is not able to provide full azimuthal coverage, due to the directional beam pattern of its elements.

Considering mutual coupling, one should expect that circular arrays would suffer more severe effects, since significant coupling can occur between elements located diametrically opposite of each other, in addition to the strong coupling between adjacent elements. However, the basic symmetry of circular arrays has been shown to offer a great ability to compensate for the effects of mutual coupling, by breaking down the array excitation into a series of symmetrical spatial components [14]. Also, this unique feature can deflect directional beams, which remain constant in

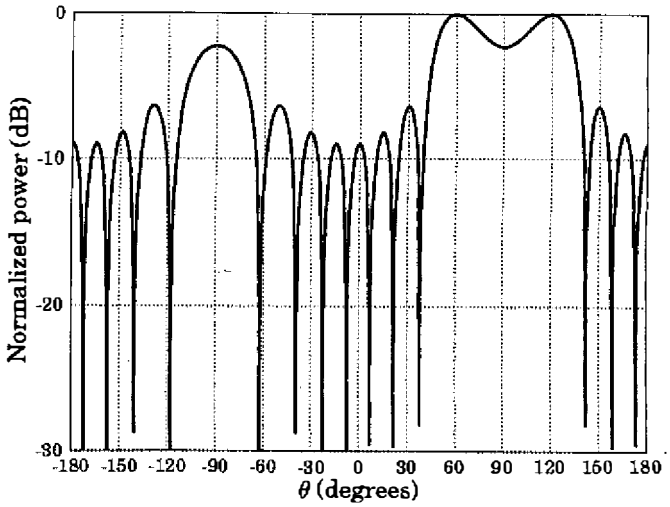

Figure 2a. The directional pattern of the simple narrowband beamformer applied to an eight-element uniform linear array with $d = \lambda/2$ and $\theta_0 = 60°$.

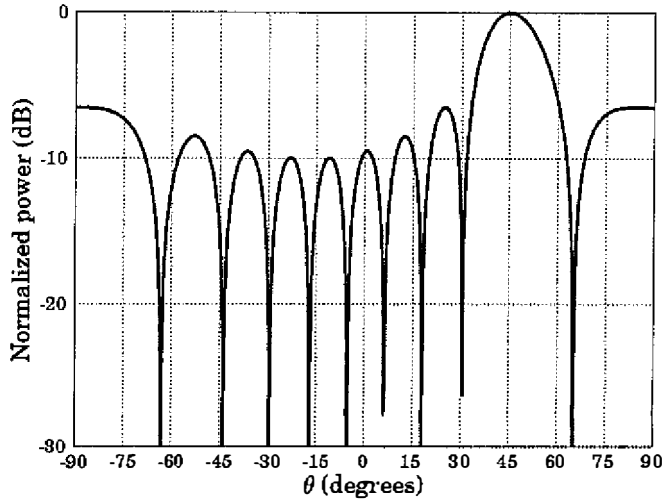

Figure 2b. The directional pattern of the simple narrowband beamformer applied to a 10-element uniform linear array with $d = \lambda/2$ and $\theta_0 = 45°$.

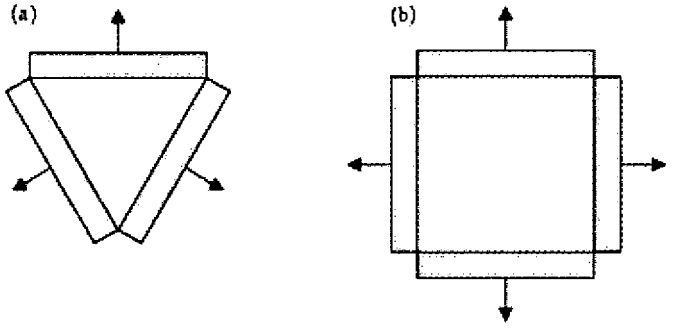

Figure 3. (a) A triangular and (b) a rectangular arrangement of the uniform linear arrays, each covering fields of view of 120° and 90°, respectively.

shape over broad bandwidths. These attractive features, along with new and more convenient methods of array phasing, give powerful advantages to circular arrays for those applications where mutual coupling can limit the performance of the antenna.

Nevertheless, the advantages of uniform circular arrays come at a cost. Many useful array-processing techniques that are derived for uniform linear arrays do not extend directly to uniform circular arrays, due to the mathematical structure of their steering vector not possessing the convenient *Vandermonde* form. (A Vandermonde vector with order n can be written in the form $\left[1, x^1, x^2, ..., x^{n-1}\right]^T$ [15]). In particular, such techniques are

- Dolph-Tschebyscheff beam pattern design [16], and
- spatial smoothing for DOA estimation [17-19].

Other problems uniform circular arrays are challenged to solve include the combating of multipath (introducing highly correlated signal paths) and *multiple access interference* (MAI) mobile environments. As a result, computationally intensive array-processing techniques that are suited for two-dimensional geometries must be employed, such as *maximum likelihood* (ML) methods [20], to deal with such environments.

Circular arrays have been used for many years in the HF band for both communications and direction finding. These systems employed beam co-phased excitation with time-delay compensation to achieve broad-bandwidth operation [21]. The elements were usually monopoles, or a combination of driven and parasitic elements.

3. Circular Array Geometry

Referring to Figure 4, let us assume that a uniform circular array with radius a and consisting of N uniformly distributed antenna elements, assumed to be identical and omnidirectional, is located on the x-y plane and is illuminated by an impinging planar wavefront. A spherical coordinate system is used to represent the arrival directions from incoming plane waves. The origin of the coordinate system is located at the center of the array. Source elevation angles, $\theta \in [0, \pi/2]$, are measured from the z axis, and azimuth angles, $\phi \in [0, 2\pi]$, are measured counterclockwise from the x axis on the x-y plane.

The angular position of the nth element of the array is given by [10]

$$\phi_n = 2\pi\left(\frac{n}{N}\right), \quad n = 1, 2, ..., N. \tag{6}$$

The narrowband planar wave with wavelength λ (and corresponding wavenumber $k = 2\pi/\lambda$) arrives at the antenna from elevation angle θ and azimuthal angle ϕ. The unit vector $\hat{\mathbf{a}}_r$ from the origin is represented in Cartesian coordinates by

$$\hat{\mathbf{a}}_r = \hat{\mathbf{a}}_x \sin\theta\cos\phi + \hat{\mathbf{a}}_y \sin\theta\sin\phi + \hat{\mathbf{a}}_z \cos\theta. \tag{7}$$

The unit vector $\hat{\mathbf{a}}_{pn}$ from the origin to the nth element of the array is written as

$$\hat{\mathbf{a}}_{pn} = \hat{\mathbf{a}}_x \cos\phi_n + \hat{\mathbf{a}}_y \sin\phi_n, \quad n = 1, 2, ..., N. \tag{8}$$

The vector $\Delta\mathbf{r}_n$ represents the differential distance by which the planar wavefront reaches the nth element of the array relative to the origin, and it is given by [10]

$$\Delta\mathbf{r}_n = \hat{\mathbf{a}}_r a \cos\psi_n. \tag{9}$$

Since the wavefront is incoming and not radiating outwards, ψ_n can be expressed as

$$\begin{aligned}
\cos\psi_n &= -\hat{\mathbf{a}}_r \cdot \hat{\mathbf{a}}_{pn} \\
&= -\left(\hat{\mathbf{a}}_x \sin\theta\cos\phi + \hat{\mathbf{a}}_y \sin\theta\sin\phi + \hat{\mathbf{a}}_z \cos\theta\right) \\
&\quad \cdot \left(\hat{\mathbf{a}}_x \cos\phi_n + \hat{\mathbf{a}}_y \sin\phi_n\right) \\
&= -\left(\sin\theta\cos\phi\cos\phi_n + \sin\theta\sin\phi\sin\phi_n\right) \\
&= -\sin\theta\left(\cos\phi\cos\phi_n + \sin\theta\sin\phi_n\right) \\
&= -\sin\theta\cos\left(\phi - \phi_n\right), \quad n = 1, 2, ..., N,
\end{aligned} \tag{10}$$

and, therefore, Equation (9) reduces to [10]

$$\Delta\mathbf{r}_n = -\hat{\mathbf{a}}_r a \sin\theta\cos\left(\phi - \phi_n\right), \quad n = 1, 2, ..., N. \tag{11}$$

Furthermore, assuming that the wavefront passes through the origin at time $t = 0$, it impinges on the nth element of the array at the relative time of

$$\tau_n = -\frac{a}{c}\sin\theta\cos\left(\phi - \phi_n\right), \quad n = 1, 2, ..., N, \tag{12}$$

where c is the speed of light in free space. Positive time delay indicates that the wavefront impinges on the nth element after it passes through the origin, whereas negative time delay indicates that the wavefront impinges on the nth element before it arrives at the origin. Moreover, based on Equation (10), the element-space circular-array *steering vector* is given by

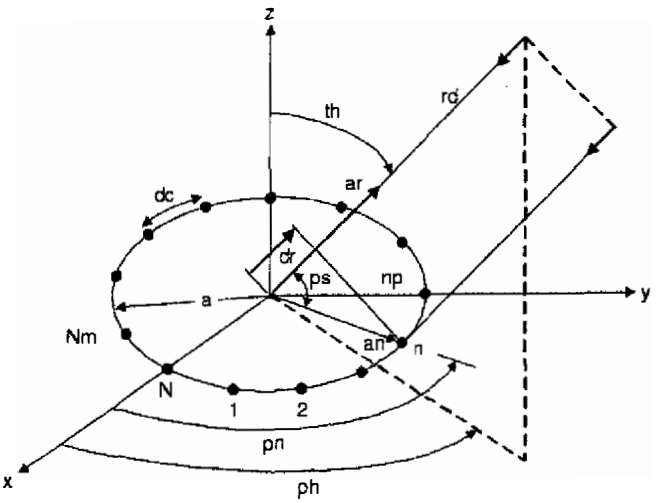

Figure 4. The geometry of a circular array with radius a and N equally spaced elements, along with an impinging planar wavefront.

$$\mathbf{a}(\boldsymbol{\theta}) = \mathbf{a}(\varsigma,\phi) = \left[e^{\varsigma\cos(\phi-\phi_1)}, e^{\varsigma\cos(\phi-\phi_2)}, \ldots, e^{\varsigma\cos(\phi-\phi_N)} \right]^T, \quad (13)$$

where the elevation dependence is through the parameter $\varsigma = ka\sin\theta$, and the vector $\boldsymbol{\theta} = (\varsigma,\phi)$ is used to represent source arrival directions.

The dominant method in analyzing circular arrays is through the so-called *phase-mode excitation*}, which is essentially the decomposition of the array excitation function into different Fourier harmonics by using Fourier analysis. It stems from the fact that the beam pattern of the uniform circular array is periodic in azimuth [21].

4. Direction-of-Arrival Estimation with Uniform Circular Arrays

In this section, we consider the computation of the *directions of arrival* (DOAs) of signals transmitted towards uniform circular arrays by several sources. So far, several algorithms have been proposed in the literature for the two-dimensional angle estimation (azimuth and elevation) of multiple plane waves incident on a uniform circular array.

4.1 Real Beam-Space MUSIC for Circular Arrays

As with other array geometries, a major category in the context of DOA estimation with uniform circular arrays relies on the *MUltiple SIgnal Classification* (MUSIC) algorithm, which utilizes the fact that signal vectors are orthogonal to the noise subspace. MUSIC offers numerous advantages over element-space operation, including reduced computation, since subspace estimates are obtained via real-valued eigen decompositions, and enhanced performance in correlated-source scenarios, due to the attendant forward-backward averaging effect [22]. An interesting version of the MUSIC algorithm is the Real Beam-space MUSIC algorithm for uniform circular arrays (UCA-RB-MUSIC). The complete development of the algorithm can be found in [22].

4.1.1 Simulation Results of Direction Finding with the UCA-RB-MUSIC Algorithm

In order to test the UCA-RB-MUSIC algorithm, we considered two examples with different array geometries and different numbers of sources, as shown in Table 1. The corresponding UCA-RB-MUSIC power spectrum for these two cases is displayed in Figures 5a and 5b, respectively. The performance of the UCA-RB-MUSIC was indeed excellent, since very sharp peaks appeared in the directions of arriving signals.

4.1.2 Comparison of Classical MUSIC with the UCA-RB-MUSIC Algorithm

The classical MUSIC algorithm is a very popular high-resolution algorithm, applicable to arrays of arbitrary but known configuration and response [23, 24]. An interesting investigation is to compare the classical MUSIC algorithm with the UCA-RB-MUSIC algorithm, developed exclusively for uniform circular arrays. To compare these two algorithms, we considered the signals and geometries of Table 2, where the impinging signals were assumed to arrive from an elevation identical to the plane of the array ($\theta = \pi/2$).

The corresponding power spectra for these two cases are shown in Figures 6a and 6b, respectively. For the first case, both of the algorithms had great performance, with that of the UCA-RB-MUSIC algorithm being slightly better (sharper peaks). This is justified by the fact that while the classical MUSIC algorithm is applicable to every possible array geometry, the UCA-RB-MUSIC was explicitly developed for uniform circular arrays, and fully exploits the array structure. However, for the second case, we observed that while the performance of the classical MUSIC was

Table 1a. The geometries used to test the UCA-RB-MUSIC algorithm.

	Case 1	Case 2
Number of elements	$N = 8$	$N = 10$
Radius of the UCA	$a = 0.6\lambda$ $(d_c = 0.4127\lambda)$	$a = 0.75\lambda$ $(d_c = 0.4712\lambda)$
Number of impinging sources	$K = 3$	$K = 4$
SNR per equal-power source	10 dB	10 dB
Number of collected samples	3000	4000

Table 1b. The directions of arrival of the signals used to test the UCA-RB-MUSIC algorithm.

Case 1	Case 2
$\theta_1 = 30°, \phi_1 = 120°$	$\theta_1 = 30°, \phi_1 = 300°$
$\theta_2 = 45°, \phi_2 = 210°$	$\theta_2 = 45°, \phi_2 = 150°$
$\theta_3 = 60°, \phi_3 = 300°$	$\theta_3 = 60°, \phi_3 = 240°$
	$\theta_4 = 75°, \phi_4 = 60°$

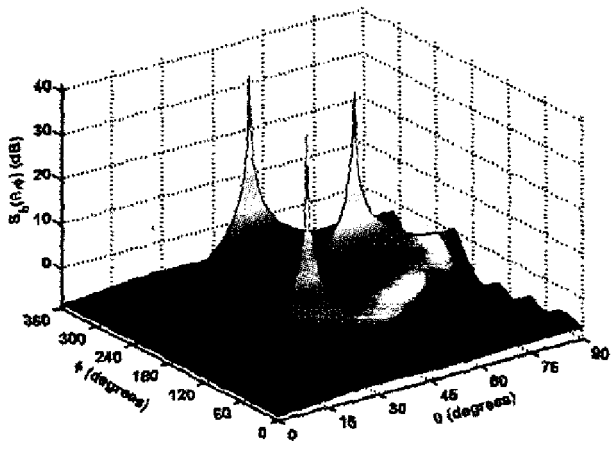

Figure 5a. The UCA-RB-MUSIC spectrum for Case 1 of Table 1.

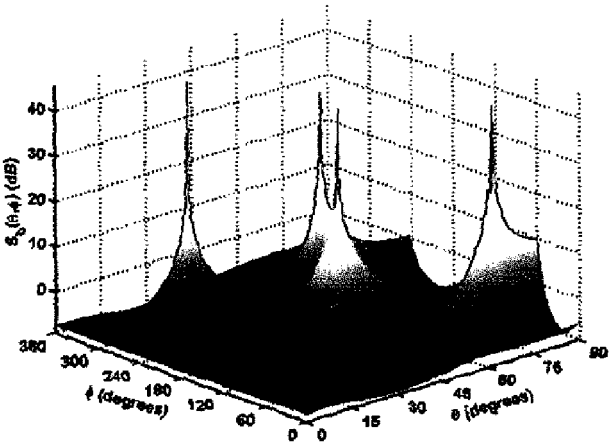

Figure 5b. The UCA-RB-MUSIC spectrum for Case 2 of Table 1.

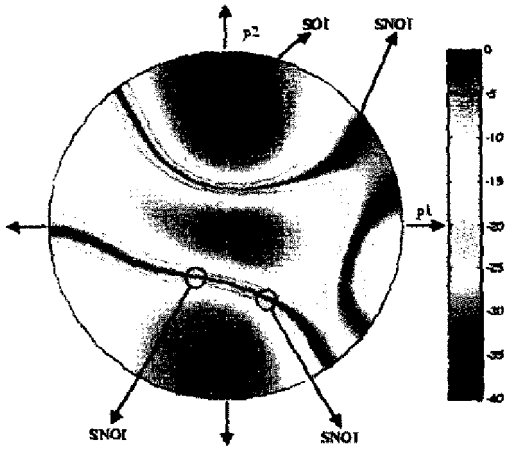

Figure 10. A contour polar radiation pattern using the geometry of Table 5 (relative power in dB down).

Table 2a. The geometries used to compare the classical MUSIC and the UCA-RB-MUSIC algorithms.

	Case 1	Case 2
Number of elements	$N = 8$	$N = 7$
Radius of the UCA	$a = 0.6\lambda$ $(d_c = 0.4127\lambda)$	$a = 0.52\lambda$ $(d_c = 0.4668\lambda)$
Number of impinging sources	$K = 3$	$K = 4$
SNR per equal-power source	10 dB	10 dB
Number of collected samples	3000	4000

Table 2b. The directions of arrival of the signals used to compare the classical MUSIC and the UCA-RB-MUSIC algorithms.

Case 1	Case 2
$\theta_1 = 90°, \phi_1 = 120°$	$\theta_1 = 90°, \phi_1 = 60°$
$\theta_2 = 90°, \phi_2 = 210°$	$\theta_2 = 90°, \phi_2 = 150°$
$\theta_3 = 90°, \phi_3 = 300°$	$\theta_3 = 90°, \phi_3 = 225°$
	$\theta_4 = 90°, \phi_4 = 330°$

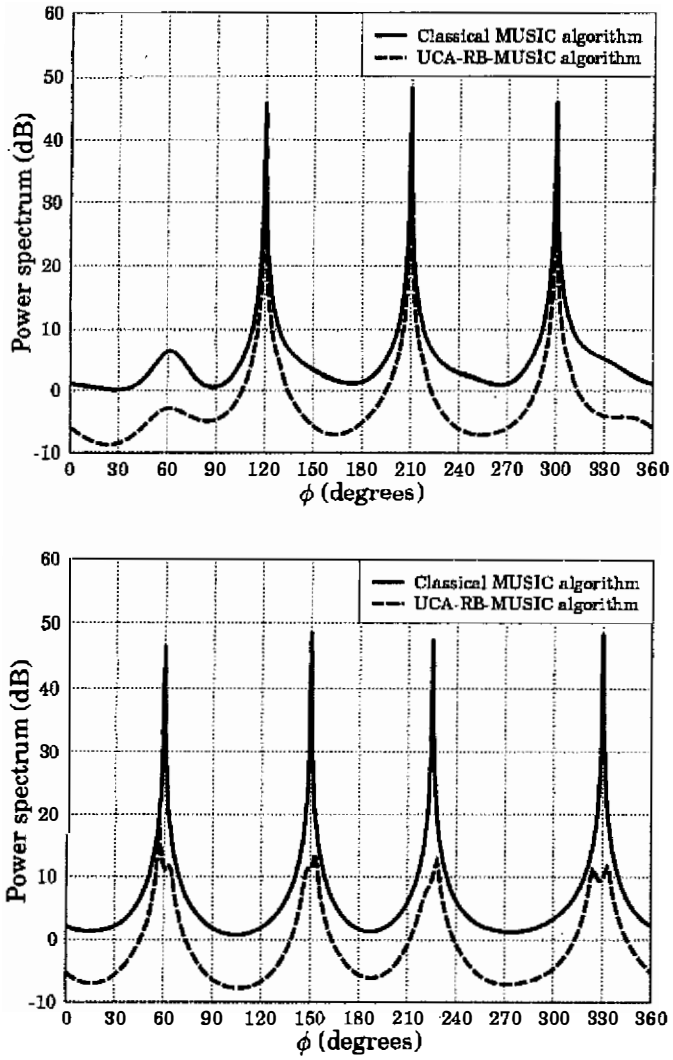

Figure 6. A comparison of the classical MUSIC and UCA-RB-MUSIC algorithms: (a, top) Case 1 of Table 2 and (b, bottom) Case 2 of Table 2.

still great, that of UCA-RB-MUSIC was very poor. Its peaks were not sharp and were misplaced. This is justified by the fact that the number of antenna elements was less than double the number of sources, which violated the requirements and assumptions for the development of the algorithm [22]. This is a significant disadvantage of the UCA-RB-MUSIC algorithm, since it can identify the directions of not more than $N/2$ sources with an N-element uniform circular array with excellent performance, compared to the classical MUSIC algorithm, which can resolve the directions of arrival from up to N sources with very adequate performance.

4.2 The UCA-ESPRIT Algorithm

Although powerful, the UCA-RB-MUSIC as well as the classical MUSIC algorithms do require a two-dimensional spectral search to obtain direction-of-arrival estimates, with significant computational complexity. However, the unitary UCA-ESPRIT algorithm, proposed by Zoltowski et al. [22], has proven to be a very powerful algorithm, as well. The UCA-ESPRIT algorithm is fundamentally different from the classical ESPRIT algorithm in the sense that the uniform circular array does not need to possess the displacement invariances required by conventional ESPRIT-based algorithms [25]. Rather, its development hinges on a recursive relationship among the Bessel functions [22]. The similarity to ESPRIT is that the eigenvalues of a matrix (which is derived from the least-square solution to an overdetermined system of equations) directly yield the direction-of-arrival estimates. UCA-ESPRIT is a novel algorithm, and the only one that provides closed-form automatically-paired source azimuth and elevation estimates. Applying ESPRIT in conjunction with uniform circular arrays, the eigenvalues of a matrix have the form $\mu_i = \sin\theta_i e^{j\phi_i}$, where θ_i and ϕ_i are the elevation and azimuthal angles of the ith impinging source, respectively. With UCA-ESPRIT, computationally intensive spectral-search procedures (as with MUSIC [26, 27]), iterative solutions, and multi-dimensional optimization problems [28] are avoided. Apparently, UCA-ESPIRT is considered superior to existing two-dimensional angle-estimation algorithms with respect to the computational requirements. Since $\sin\theta = \sin(180° - \theta)$, a profound ambiguity arises for the correct detection of the elevation angle. This can be easily solved by restricting the visible region to the half space ($0 \le \theta \le \pi/2$), typical to a wireless communication system. The complete analysis of the algorithm can also be found in [22].

4.2.1 Simulation Results of Direction Finding with the UCA-ESPRIT Algorithm

Using the UCA-ESPRIT algorithm, simulation results gave very accurate results in simultaneously finding both the elevation

and azimuth directions of arrival for different sources transmitting signals towards the array. A very impressive feature of the algorithm, which reveals its robustness, was its great performance in environments where the noise power was dominant over that of the signals. For example, keeping all the parameters of the simulations the same (array configuration, power and angle of the uncorrelated sources, and number of samples), and altering only the variance of the AWGN (additive white Gaussian noise) present, we observed relatively insignificant deviation from the exact directions of arrival for high-noise variances. Extensive experiments verified our argument. In Table 3, the same scenario for different SNR values was repeated for an adequate number of Monte Carlo simulations each time, and the elevation and azimuthal angle from each source was estimated as the mean of the outcome from all tests. We observed very exact direction-of-arrival estimations, even for noise powers 10 times higher than that of each signal. Finally, for the extraordinary scenario of $SNR = -20$ dB, the difference between the estimated and the exact directions of arrival came out to be only a few degrees, however with significant standard deviation.

5. Adaptive Beamforming with Uniform Circular Arrays

There are several algorithms applicable to circular arrays that perform adaptive-beamforming techniques, some of them already reviewed [29]. One of the simplest algorithms, and one of the most commonly used to adapt the amplitude and phase excitation of the antenna elements, is the *least mean squares* (LMS) algorithm [30, 31]. During the adaptive process, an injected pilot signal simulates a received signal from a desired look direction [32]. This allows the array to be trained, so that its directional pattern has a main lobe in the previously specified look direction. At the same time, the signal-processing unit can reject any incident interference with an angle of propagation different from that of the desired signal. Through minimizing the mean square error between an a priori known training sequence and the signal received at the receiver, the complex excitation weights are updated at each iteration until stability is achieved. The entire process leads to a maximum of the antenna-directivity pattern towards the direction of the desired signal, and appropriate nulls are formed at the angles of interference. The least mean squares is a low-complexity algorithm and, thus, can be easily used in real-time applications. Other adaptive algorithms that may be applied affectively are the *recursive least square* (RLS) [9, 33], the *conjugate gradient* (GC) [34], the *constant modulus* (CM) [35], and the *decision-directed* (DD) [36] algorithms.

To examine the applicability of adaptive algorithms with uniform circular arrays, we first considered the case where only a signal of interest was present. With this scenario, we compared the classical and adaptive beamforming methods. The antenna pattern formed using the weight vector $\mathbf{w}_b = \mathbf{a}(\boldsymbol{\theta}_0)$, where $\mathbf{a}(\boldsymbol{\theta})$ is given by Equation (13), has its maximum gain towards the desired direction θ_0, ϕ_0, compared to any other weight vector of the same magnitude, and it is referred to as *classical beamforming* [10]. Mathematically, this can be justified by the Cauchy-Schwartz inequality

$$\left|\mathbf{w}^H(\theta)\mathbf{a}(\boldsymbol{\theta}_0)\right|^2 \le \|\mathbf{w}\|^2 \left\|\mathbf{a}(\theta_0)\right\|^2 \qquad (14)$$

for all vectors $\mathbf{w}$, with equality holding if and only if $\mathbf{w}$ is proportional to $\mathbf{a}(\boldsymbol{\theta}_0)$ [37]. Alternatively, this weight vector can be found by appropriately employing an adaptive algorithm, assuming that a single source is exciting the array.

Table 3a. The geometry used to evaluate the performance of the UCA-ESPIRT algorithm.

Number of elements	$N = 12$
Radius of the UCA	$a = 0.8\lambda$ ($d_c = 0.4189\lambda$)
Number of impinging sources	$K = 3$
Number of collected samples	3000
Number of Monte Carlo simulations	100

Table 3b. The directions of arrival of the signals used to evaluate the performance of the UCA-ESPIRT algorithm.

Exact	
$\theta_1 = 15°$	$\phi_1 = 150°$
$\theta_2 = 30°$	$\phi_2 = 210°$
$\theta_3 = 45°$	$\phi_3 = 330°$
SNR per equal-power source: +10 dB	
$\theta_1 = 15.0010°$, std. = 0.0276°	$\bar{\phi}_1 = 150.0066°$, std. = 0.1387°
$\theta_2 = 30.0159°$, std. = 0.0390°	$\bar{\phi}_2 = 209.9967°$, std. = 0.0528°
$\theta_3 = 45.2591°$, std. = 0.0558°	$\bar{\phi}_3 = 329.9947°$, std. = 0.0465°
SNR per equal-power source: 0 dB	
$\theta_1 = 15.0123°$, std. = 0.0826°	$\bar{\phi}_1 = 149.9263°$, std. = 0.4770°
$\theta_2 = 30.0112°$, std. = 0.1277°	$\bar{\phi}_2 = 210.0069°$, std. = 0.1724°
$\theta_3 = 45.3177°$, std. = 0.1614°	$\bar{\phi}_3 = 329.9940°$, std. = 0.1623°
SNR per equal-power source: −10 dB	
$\theta_1 = 14.9395°$, std. = 0.3275°	$\bar{\phi}_1 = 149.8370°$, std. = 1.9409°
$\theta_2 = 30.0713°$, std. = 0.5320°	$\bar{\phi}_2 = 210.1875°$, std. = 0.8380°
$\theta_3 = 45.2124°$, std. = 0.7346°	$\bar{\phi}_3 = 330.0246°$, std. = 0.7250°
SNR per equal-power source: −20 dB	
$\theta_1 = 15.2311°$, std. = 4.4905°	$\bar{\phi}_1 = 143.1731°$, std. = 28.8028°
$\theta_2 = 27.4981°$, std. = 5.2720°	$\bar{\phi}_2 = 209.1216°$, std. = 12.1141°
$\theta_3 = 42.7270°$, std. = 6.3526°	$\bar{\phi}_3 = 329.2504°$, std. = 11.0682°

For this comparison, we considered a uniform circular array with $d_c = \lambda/2$ and $N = 8$ isotropically radiating elements ($a = 4\lambda/2\pi$). To obtain the appropriate weight vector adaptively, we assumed an SNR of 10 dB, and employed the least-mean-squares algorithm with step size $\mu = 0.001$. Figure 7a shows the resulting beam pattern with respect to ϕ for $\theta = 90°$ ($\theta_0 = 90°$, $\phi_0 = 90°$), and Figure 7b shows the resulting beam pattern with respect to θ for $\phi = 0°$ ($\theta_0 = 45°$, $\phi_0 = 0°$). We observed that the beam patterns with respect to both ϕ and θ are almost identical with the classical and adaptive beamforming technique. This revealed that for the case of a signal of interest only, the adaptive beamforming technique and the classical technique are approximately the same. Figures 7c and 7d show the amplitude and phase excitations, respectively, for both classical and adaptive beamforming that resulted in the beam pattern of Figure 7a, whereas Figures 7e and 7f show the amplitude and phase excitations, respectively, for both the classical and adaptive beamforming that

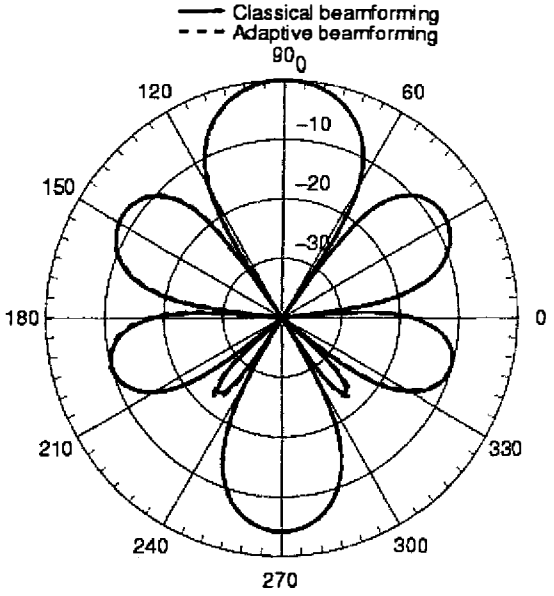

Figure 7a. A comparison of the classical and adaptive beamforming method with a single signal of interest: the beam pattern with respect to ϕ for $\theta = 90°$ ($\theta_0 = 90°$, $\phi_0 = 90°$).

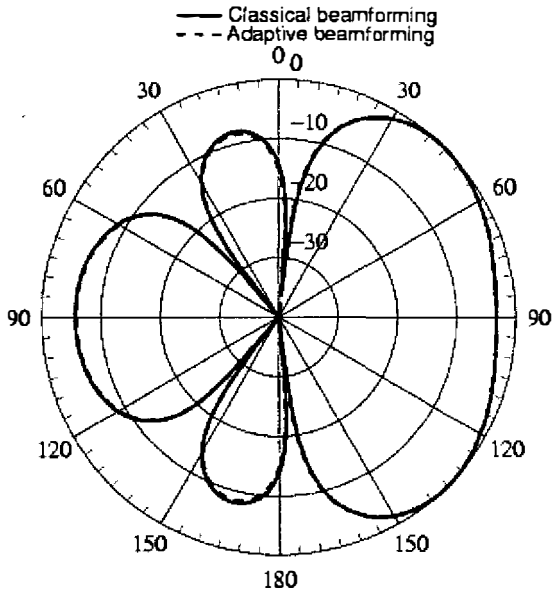

Figure 7b. A comparison of the classical and adaptive beamforming method with a single signal of interest: the beam pattern with respect to θ for $\phi = 0°$ ($\theta_0 = 45°$, $\phi_0 = 0°$).

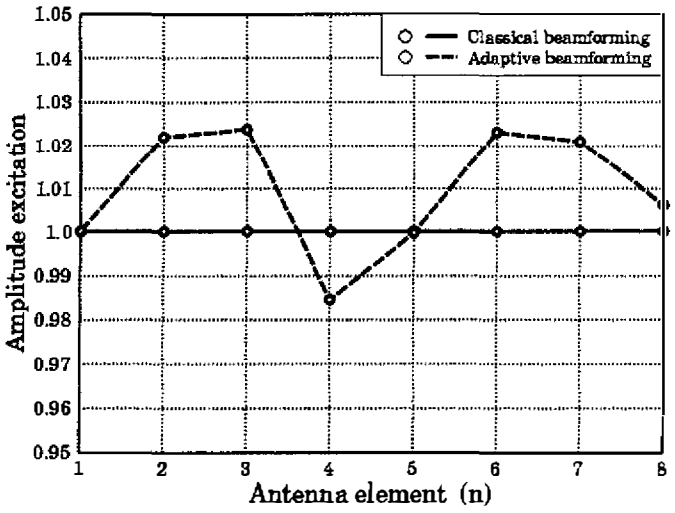

Figure 7c. A comparison of the classical and adaptive beamforming method with a single signal of interest: The amplitude excitation for each element of the circular array for classical and adaptive beamforming along azimuth (Figure 7a).

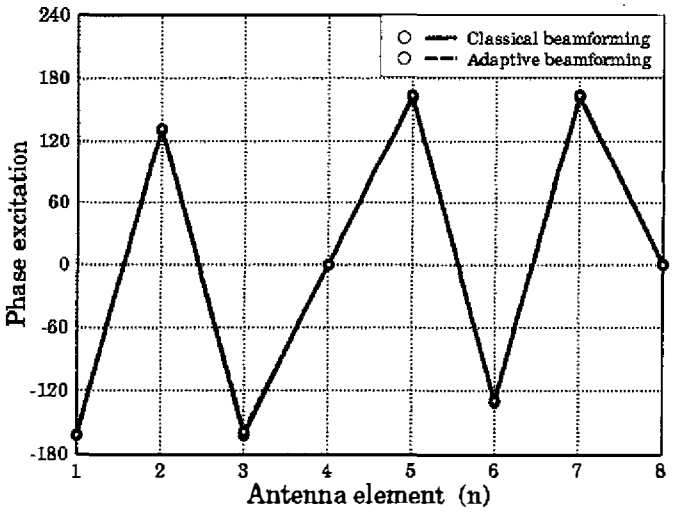

Figure 7d. A comparison of the classical and adaptive beamforming method with a single signal of interest: The phase excitation for each element of the circular array for classical and adaptive beamforming along azimuth (Figure 7a).

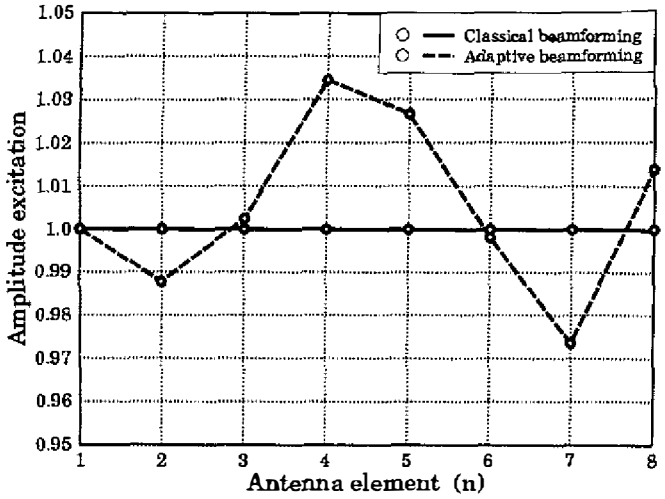

Figure 7e. A comparison of the classical and adaptive beamforming method with a single signal of interest: The amplitude excitation for each element of the circular array for classical and adaptive beamforming along elevation (Figure 7b).

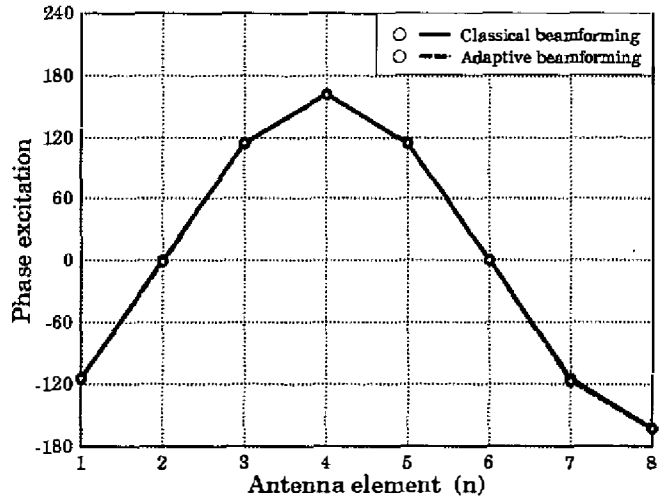

Figure 7f. A comparison of the classical and adaptive beamforming method with a single signal of interest: The phase excitation for each element of the circular array for classical and adaptive beamforming along elevation (Figure 7b).

Table 4a. The geometries used to study one-dimensional adaptive beamforming with uniform circular arrays employing the least-mean-squares algorithm.

Number of elements	$N = 8$ isotropic
Radius of the UCA	$a = 2\pi/\lambda$ $(d_c = 0.5\lambda)$
Number of impinging sources	$K = 4$
SNR per equal-power source	10 dB
Number of collected samples	1500

Table 4b. The directions of arrival of the signals used to study one-dimensional adaptive beamforming with uniform circular arrays employing the least-mean-squares algorithm.

	Case 1	Case 2
Signal of interest	$\theta_1 = 60°, \phi_1 = 0°$	$\theta_1 = 45°, \phi_1 = 0°$
Signals not of interest	$\theta_2 = 60°, \phi_2 = 90°$	$\theta_2 = 15°, \phi_2 = 0°$
	$\theta_3 = 60°, \phi_3 = 300°$	$\theta_3 = 75°, \phi_3 = 0°$

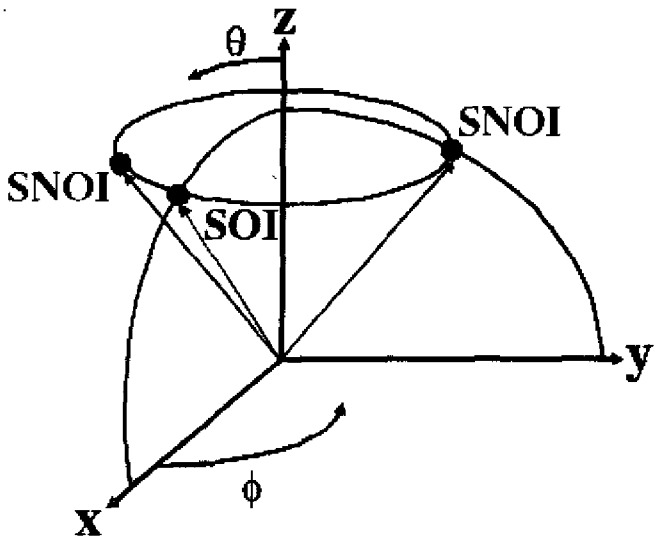

Figure 8a. One-dimensional adaptive beamforming along the azimuth for fixed elevation.

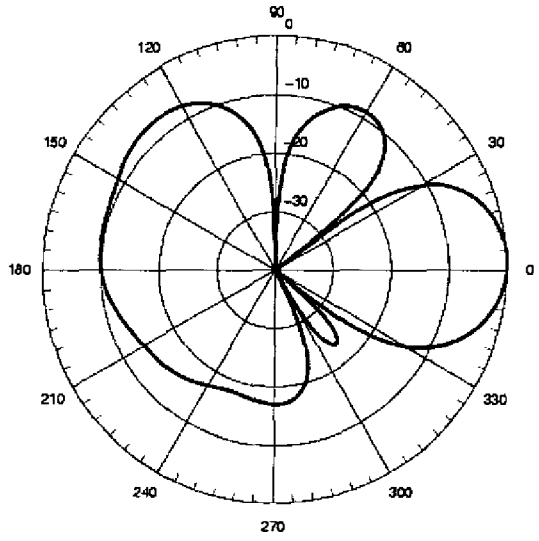

Figure 8b. The radiation pattern with respect to ϕ for fixed $\theta = 60°$ (Case 1 of Table 4) resulting from one-dimensional adaptive beamforming along the azimuth for fixed elevation.

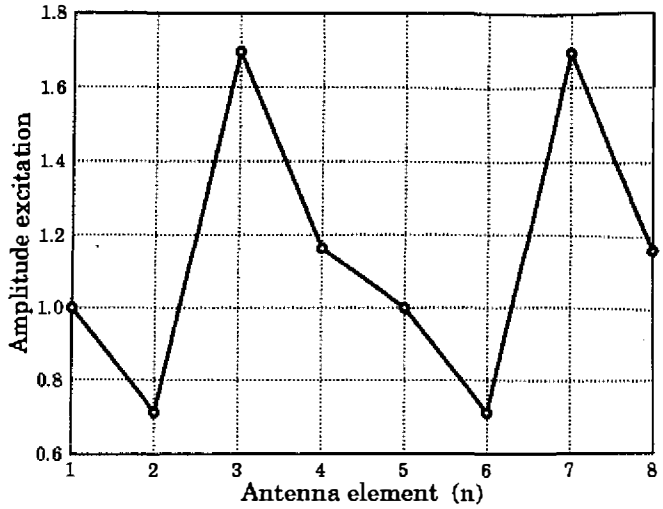

Figure 8c. The amplitude excitation for each element of the circular array required to obtain the desired beam pattern of Figure 8b.

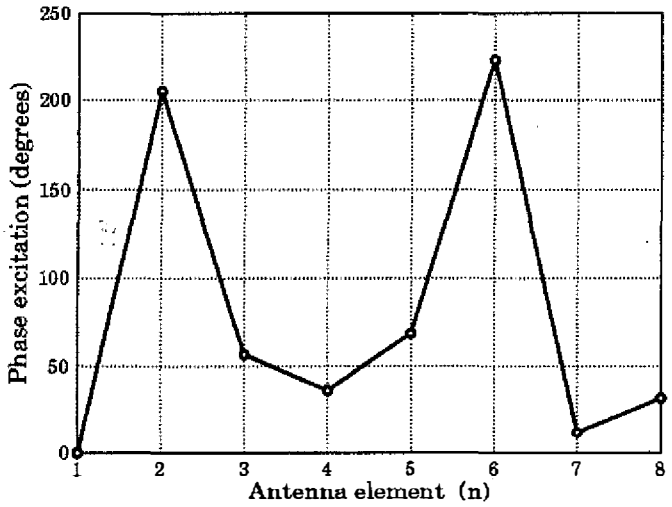

Figure 8d. The phase excitation for each element of the circular array required to obtain the desired beam pattern of Figure 8b.

resulted in the beam pattern of Figure 7b. Not surprisingly, the amplitude and phase excitations of the antenna elements were almost identical for the classical and adaptive beamforming method, for the radiation patterns with respect to both ϕ and θ.

5.1 One-Dimensional Adaptive Beamforming

When only a signal of interest is assumed, both the classical and adaptive beamforming methods can be applied. However, when both signals of interest and signals not of interest are simultaneously present, the classical method cannot be used. Thus, to accomplish beamforming in that situation, we have to resort to the adaptive technique. To show the ability of adaptive algorithms to direct the maximum towards the signal of interest and nulls towards the signals not of interest, we first consider the case of one-dimensional beamforming, i.e., beamforming along the azimuth while keeping the elevation constant, and vice versa. For the simulation process, we considered the geometry and signals of Table 4, with the use of the least-mean-squares algorithm with step size $\mu = 0.001$. Furthermore, for each beamforming example in this paper the signals from the radiating sources were assumed to be equal-power, stationary, zero-mean, uncorrelated random processes. Moreover, uncoded BPSK (binary phase-shift keying) modulation information bits were be used to simplify the simulations.

As a first example, we chose to perform adaptation along the azimuth for signals arriving from a fixed elevation, as described by Case 1 of Table 4, and illustrated in Figure 8a. Figure 8b shows the beam pattern of the circular array at the end of the adjustment process for the *signal of interest* (SOI) and *signals not of interest* (SNOIs) imposed in the design. Figures 8c and 8d illustrate the corresponding normalized amplitude and phase excitations, respectively, of each element of the array, that resulted at the end of the adaptation and led to the desired radiation pattern of Figure 8b.

Using the same uniform circular array, Figure 9b illustrates another example of a beam pattern at the end of the adjustment process for beamforming that this time was performed along the elevation, i.e., for a fixed azimuth, as described by Case 2 of Table 4 and illustrated in Figure 9a. Because of the angular proximity of the two signals not of interest to the signal of interest in this example, the beam pattern maximum did not focus exactly on the direction of the signal of interest ($\theta = 45°$, $\phi = 0°$) at the convergence of the adaptive algorithm. It was shifted a few degrees less in the θ direction ($\approx 38°$ instead of 45°). An intuitive explanation for this loss in performance is that the uniform circular array was not as sensitive to signals arriving from directions varying in elevation, rather than in azimuth, because it was oriented on a plane with fixed elevation and its elements were located at dif-

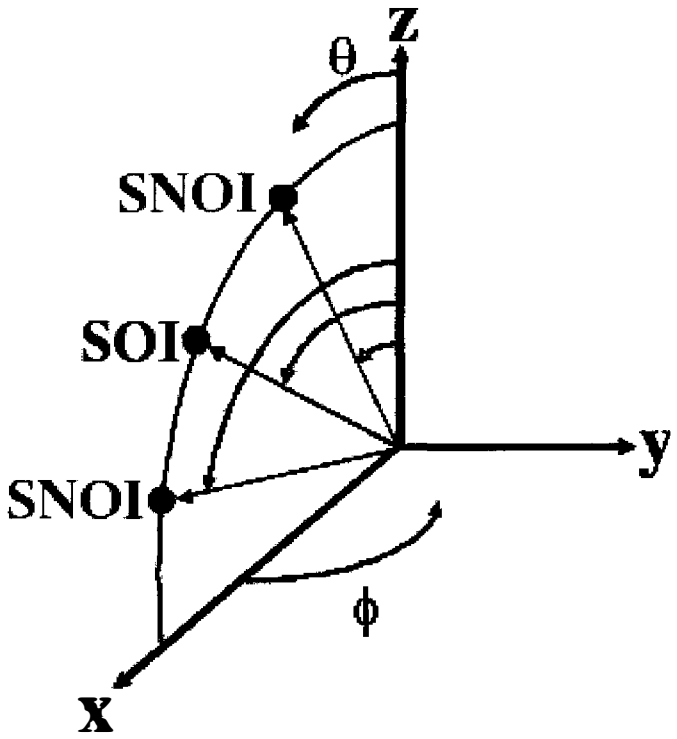

Figure 9a. One-dimensional adaptive beamforming along elevation for fixed azimuth.

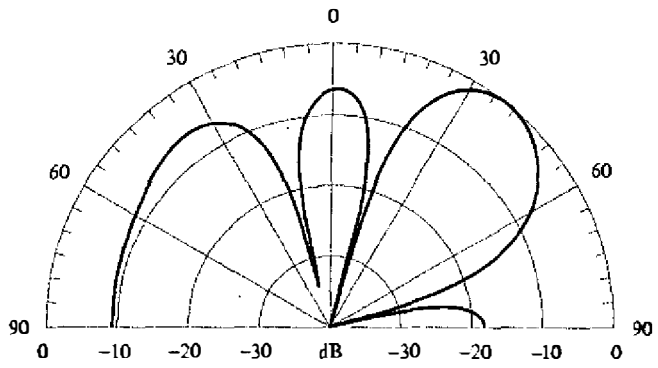

Figure 9b. The radiation pattern with respect to θ for fixed $\phi = 0°$ (Case 2 of Table 4) resulting from one-dimensional adaptive beamforming along elevation for fixed azimuth.

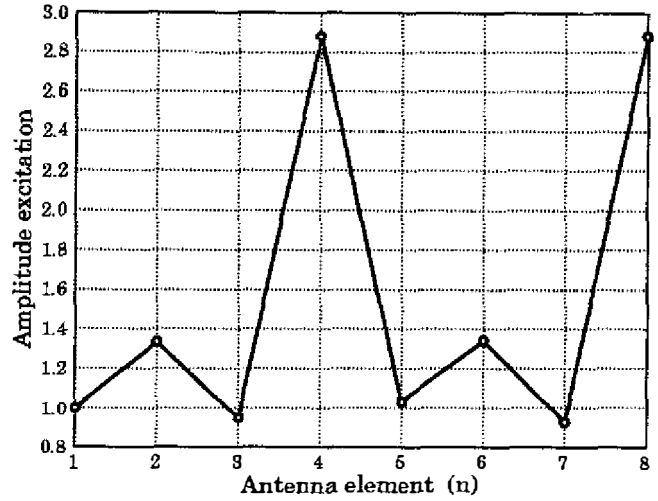

Figure 9c. The amplitude excitation for each element of the circular array required to obtain the desired beam pattern of Figure 9b.

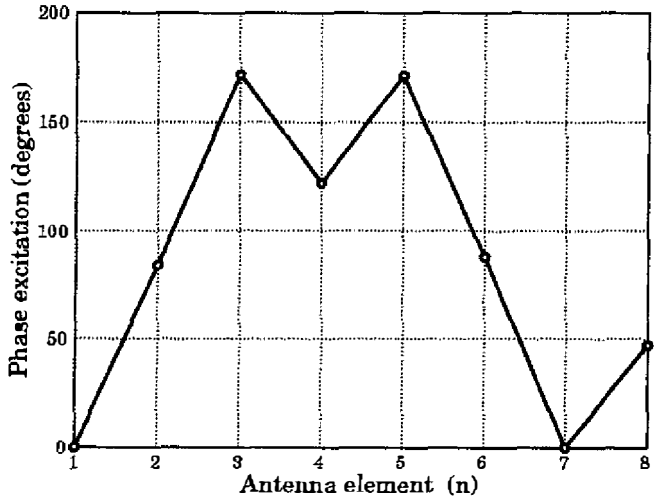

Figure 9d. The phase excitation for each element of the circular array required to obtain the desired beam pattern of Figure 9b.

Table 5a. The geometries used to study two-dimensional adaptive beamforming with uniform circular arrays employing the least-mean-squares algorithm.

Number of elements	$N = 8$ isotropic
Radius of the UCA	$a = 2\pi/\lambda$ $(d_c = 0.5\lambda)$
Number of impinging sources	$K = 4$
SNR per equal-power source	10 dB
Number of collected samples	2500

Table 5b. The directions of arrival of the signals used to study two-dimensional adaptive beamforming with uniform circular arrays employing the least-mean-squares algorithm.

Signal of interest	$\theta_1 = 60°, \phi_1 = 90°$
Signals not of interest	$\theta_2 = 75°, \phi_2 = 30°$
	$\theta_3 = 30°, \phi_3 = 240°$
	$\theta_4 = 45°, \phi_4 = 300°$

ferent angles in azimuth. The corresponding normalized amplitude and phase excitation, respectively, of each element of the array that resulted at the end of the adjustment process are plotted in Figures 9c and 9d, respectively. A careful observation of Figures 9c and 9d indicated that both the amplitude and phase excitation of the elements symmetrically about the fourth element with $\phi_4 = 180°$ (or, equivalently, the eighth element with $\phi_8 = 360°$) were approximately the same. This was expected, since the adaptive beamforming was performed for $\phi = 0°$ – equivalently, on the x-z plane – and the elements that were symmetrical about the x axis experienced exactly the same phase difference.

5.2 Two-Dimensional Adaptive Beamforming

In the previous adaptation, we examined the capability of the uniform circular array to direct its maximum and to place nulls in its radiation pattern along either azimuth or elevation, only. We now examine the case of two-dimensional adaptive beamforming, where the source arrival directions can take arbitrary values in azimuth and elevation.

For the simulation process, we considered the geometry and signals of Table 5 with use of the least-mean-squares algorithm with step size $\mu = 0.001$ and all the previous assumptions about the nature of the signals. Figure 10 shows the resulting normalized radiation pattern in a polar contour representation. (A contour plot is a graphical technique for representing a three-dimensional surface by plotting constant z slices, called contours, on a two-dimensional format. That is, given a value for z, lines are drawn connecting the (x, y) coordinates where that z value occurs [38].)

It can be shown from Figure 10 that the uniform circular array possesses very satisfactory two-dimensional beamforming abilities, since the maximum and deep nulls in the pattern are formed in the directions of the signal of interest and all signals not of interest, respectively. Of course, better behavior in two-dimensional beamforming can be expected if the array possesses addi-

Table 6a. The geometries used to compare one-dimensional and two-dimensional adaptive beamforming with uniform circular arrays employing the least-mean-squares algorithm.

Number of elements	$N = 8$ isotropic
Radius of the UCA	$a = 2\pi/\lambda$ $(d_c = 0.5\lambda)$
Number of impinging uncorrelated sources	$K = 4$
SNR per equal-power source	10 dB
Number of collected samples	2000
Number of Monte Carlo simulations	200

Table 6b. The directions of arrival of the signals used to compare one-dimensional and two-dimensional adaptive beamforming with uniform circular arrays employing the least-mean-squares algorithm.

	Case 1	Case 2
Signal of interest	$\theta_1 = 90°, \phi_1 = 90°$	$\theta_1 = 60°, \phi_1 = 90°$
Signals not of interest	$\theta_2 = 60°, \phi_2 = 30°$	$\theta_2 = 75°, \phi_2 = 30°$
	$\theta_3 = 90°, \phi_3 = 240°$	$\theta_3 = 30°, \phi_3 = 240°$
	$\theta_4 = 90°, \phi_4 = 300°$	$\theta_4 = 45°, \phi_4 = 300°$

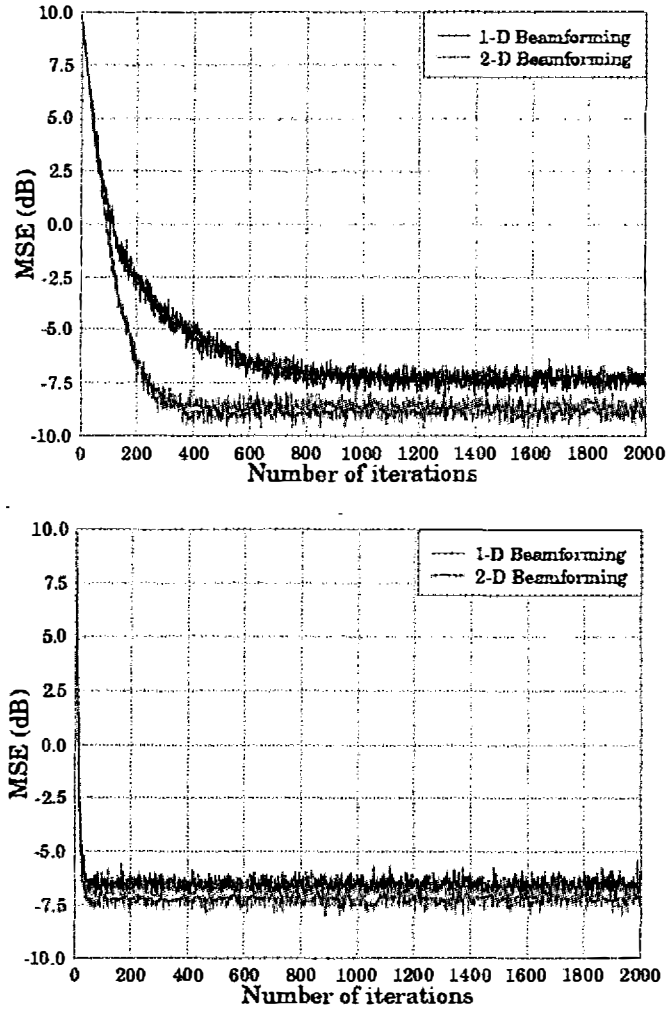

Figure 11. The mean square errors of the least-mean-squares algorithm for both cases of Table 6: (a, top) step size $\mu = 0.001$ and (b) step size $\mu = 0.01$.

tional degrees of freedom in elevation, i.e., a three-dimensional array, such as a cylindrical or spherical array.

5.3 Comparison of One-Dimensional and Two-Dimensional Adaptive Beamforming

Since the performance of the least-mean-squares adaptive algorithm has been shown to be very effective for both the one-dimensional and two-dimensional beamforming cases, an interesting comparison would be to compare the convergence behavior of the least mean squares when keeping the parameters of the system fixed, and changing only the dimensionality of the beamforming. For this purpose, we considered the geometry and signals of Table 6. The corresponding mean square errors (MSE) of the least-mean-squares algorithm with respect to the iteration number for both cases of Table 6 for $\mu = 0.001$ and $\mu = 0.01$ are shown in Figures 11a and 11b, respectively.

Concerning the least-mean-squares algorithm with the same beamforming dimensionality, the algorithm converges more slowly but with smaller mean square error towards convergence if the step size is smaller, i.e., for $\mu = 0.001$ compared to $\mu = 0.01$, which is a known behavior of the least-mean-squares algorithm. Furthermore, it is useful to notice that for the same step size of μ, the least-mean-squares algorithm achieved a slightly smaller mean square error value at its convergence for the two-dimensional beamforming case compared to the one-dimensional case; with a smaller step size, $\mu = 0.001$, this difference in mean square error values was more significant. An intuitive explanation for this behavior of the least-mean-squares algorithm stems from the time delays between the antenna elements for the one-dimensional and two-dimensional beamforming cases. For both beamforming scenarios, the corresponding sources had the same azimuthal locations, resulting in the same delays between the elements due to azimuthal dependence. However, since for the one-dimensional beamforming scenario all the sources were assumed to be coplanar with the array ($\theta = 90°$) but for the two-dimensional beamforming scenario from elevation angles of less than 90°, the time delays between the antenna elements due to elevation dependence resulting from corresponding sources were larger for the one-dimensional case, according to Equation (12). Therefore, the least-mean-squares algorithm had to adjust to larger phase shifts from element-to-element in the one-dimensional beamforming scenario compared to the two-dimensional beamforming scenario, which justifies this difference in the mean square error values achieved at the end of the adjustment process.

6. Conclusions

This paper investigated uniform circular arrays for smart antennas. The two main issues related to smart antennas – estimation of the direction of arrival from incoming signals and beamforming – were both examined with the use of uniform circular arrays.

Two different approaches were considered for direction-of-arrival estimation. In the first approach, a modified version of the MUSIC algorithm, the UCA-RB-MUSIC, was applied. Simulation results showed sharper peaks in the associated spatial spectrum compared to the classical MUSIC, provided that the number of emitting sources did not exceed half the number of array elements.

This can be attributed to the fact that the UCA-RB-MUSIC has been developed exclusively for uniform circular arrays and fully exploits the symmetry the geometry possesses, whereas the classical MUSIC is applicable to arbitrary arrays of known response. However, for a number of sources exceeding half the number of array elements, the performance of the UCA-RB-MUSIC was shown to be poor, and, therefore, the use of the classical MUSIC, which can resolve satisfactory directions of arrival from a number of sources up to the number of antenna elements, is suggested.

The other approach for direction-of-arrival estimation examined in this paper was the UCA-ESPRIT algorithm, a novel algorithm that provides closed-form automatically-paired source azimuth and elevation estimates. Directions of arrival estimated through simulation results were shown to be impressively accurate compared to the exact directions of arrival, even for scenarios in which the noise power was dominant over that of the incoming signals.

Concerning beamforming, the uniform circular array was shown to have excellent beamforming capabilities in directing the maximum towards the direction of the signal of interest and deep nulls towards the directions of the signals not of interest. However, some deficiency with beamforming along elevation using uniform circular arrays was observed, and this can be justified by the fact that the uniform circular array in our simulations was located on the x-y plane. Apparently, better results should be expected with an array possessing additional degrees of freedom along elevation, a three-dimensional such as a cylindrical or spherical array.

7. Acknowledgement

The authors would like to thank the Cyprus Fulbright Commission and the National Science Foundation, under Grant No. 0355255, for the support of this work.

8. References

1. C. Sun, A. Hirata, T. Ohira, and N. C. Karmakar, "Fast Beamforming of Electronically Steerable Parasitic Array Radiator Antennas: Theory and Experiment," *IEEE Transactions on Antennas and Propagation*, **AP-52**, 7, July 2004, pp. 1819-1832.

2. "Smart Antennas," CDMA Development Group, 2004; available at http://www.cdg.org/technology/cdma_technology/smart_antennas/index.asp

3. A. O. Boukalov and S. G. Häggman, "System Aspects of Smart-Antenna Technology in Cellular Wireless Communications: An Overview," *IEEE Transactions on Microwave Theory and Techniques*, **MTT-48**, 6, June 2000, pp. 919-929.

4. J. C. Liberti and T. S. Rappaport, *Smart Antennas for Wireless Communications: IS-95 and Third Generation CDMA Applications*, Upper Saddle River, NJ, Prentice Hall, 1999.

5. G. V. Tsoulos, "Smart Antennas for Mobile Communication Systems: Benefits and Challenges," *Electron. Comm. Eng. J.*, **11**, 2, April 1999, pp. 84-94.

6. M. C. Vanderveen, *Estimation of Parametric Channel Models in Wireless Communications Networks*, PhD dissertation, Stanford University, Department of Scientific Computing and Computational Mathematics, November 1997.

7. R. Ramanathan and J. Redi, "A Brief Overview of Ad Hoc Networks: Challenges and Directions," *IEEE Communications Magazine*, **40**, 5, May 2002, pp. 20-22.

8. S. Bellofiore, J. Foutz, J. Govindarajula, Israfil Bahçeci, C. A. Balanis, A. S. Spanias, J. M. Capone, and T. M. Duman, "Smart Antenna System Analysis, Integration and Performance for Mobile Ad-Hoc Networks (MANETs)," *IEEE Transactions on Antennas and Propagation*, **AP-50**, 5, May 2002, pp. 571-581.

9. B. D. Van Veen and K. Buckley, "Beamforming: A Versatile Approach to Spatial Filtering," *IEEE Acoustics, Speech, and Signal Processing Magazine*, **5**, April 1988, pp. 4-24.

10. C. A. Balanis, *Antenna Theory: Analysis and Design, Third Edition*, New York, Wiley, 2005.

11. J. Y.-L. Chou, *An Investigation on the Impact of Antenna Array Geometry on Beamforming User Capacity*, Master's thesis, Queen's University, Kingston, Ontario, March 2002.

12. B. K. Lau, *Applications of Adaptive Antennas in Third Generation Mobile Communication Systems*, PhD dissertation, Curtin University of Technology, Australian Telecommunications Research Institute, November 2002.

13. R. H. Morelos-Zaragoza and M. Ghavami, "Combined Beamforming and Space-Time Block Coding for High-Speed Wireless Indoor Communications," in Fourth International Symposium on Wireless Personal Multimedia Communications, Aalborg, Denmark, September 2001, pp. 1427-1431.

14. C. M. Tan, P. Fletcher, M. A. Beach, A. R. Nix, M. Landmann, and R. S. Thomä, "On the Application of Circular Arrays in Direction Finding Part II: Experimental Evaluation on SAGE with Different Circular Arrays," in 1st Annual COST 273 Workshop, Espoo, Finland, May 2002, pp. 29-30.

15. http://mathworld.wolfram.com

16. C. L. Dolph, "A Current Distribution for Broadside Arrays Which Optimizes the Relationship Between Beam Width and Side-Lobe Level," *Proc. IRE*, **34**, June 1946, pp. 335-348.

17. J. E. Evans, J. R. Johnnson, and D. F. Sun, "Application of Advanced Signal Processing Angle-Of-Arrival Estimation in ATC Navigation And Surveillance Systems," MIT Lincoln Lab, Lexington, MA, Tech. Rep. 582, 1982.

18. S. U. Pillai and B. H. Kwon, "Forward/Backward Spatial Smoothing Techniques for Coherent Signal Identification," *IEEE Transactions on Acoustics, Speech, and Signal Processing*, **37**, 1, January 1989, pp. 8-15.

19. R. T. Williams, S. Prasad, A. K. Mahalanabis, and L. H. Sibul, "An Improved Spatial Smoothing Technique for Bearing Estimation in a Multipath Environment," *IEEE Transactions on Acoustics, Speech, and Signal Processing*, **36**, 4, April 1988, pp. 425-432.

20. H. Krim and M. Viberg, "Two Decades of Array Signal Processing Research: The Parametric Approach," *IEEE Signal Processing Magazine*, **13**, 4, July 1996, pp. 67-94.

21. D. E. N. Davies, *The Handbook of Antenna Design, Volume 2*, Stevenage, Steven Peregrinus, 1983, Chapter 12, pp. 299-329.

22. C. P. Mathews and M. D. Zoltowski, "Eigen-Structure Techniques for 2-D Angle of Arrival with Uniform Circular Arrays," *IEEE Transactions on Signal Processing*, **42**, 9, September 1994, pp. 2395-2407.

23. R. O. Schmidt, *A Signal Subspace Approach to Multiple Emitter Location and Spectral Estimation*, PhD dissertation, Stanford University, 1981.

24. G. Bienvenu and L. Kopp, "Principle de la Goniometrie Passive Adaptive," in Proc. 7' eme Colloque GRESIT, Nice, France, 1979, pp. 106/1-106/10.

25. R. H. Roy, *ESPRIT – Estimation of Signal Parameters via Rotational Invariance Techniques*, PhD dissertation, Stanford University, 1987.

26. R. Schmidt, "Multiple Emitter Location and Signal Parameter Estimation," *IEEE Transactions on Antennas and Propagation*, **AP-34**, 3, March 1986, pp. 276-280.

27. M. P. Clark and L. L. Scharf, "A Maximum Likelihood Estimation Technique for Spatial-Temporal Modal Analysis," 19th Asilomar Conference on Signals, Systems and Computers, November 1991, pp. 257-261.

28. A. L. Swindlehurst and T. Kailath, "Azimuth/Elevation Direction Finding Using Regular Array Geometries," *IEEE Transactions on Aerospace Electronic Systems*, **29**, 1, January 1993, pp. 145-156.

29. J. Foutz, A. Spanias, S. Bellofiore, and C. A. Balanis, "Adaptive Eigen-Projection Beamforming Algorithms for 1-D and 2-D Antenna Arrays," *IEEE Antennas and Wireless Propagation Letters*, **2**, 2003, pp. 62-65.

30. S. Haykin, *Adaptive Filter Theory*, Englewood Cliffs, NJ, Prentice Hall, 1996.

31. P. S. R. Diniz, *Adaptive Filtering: Algorithms and Practical Implementations*, Boston, MA, Kluwer Academic Publishers, 1997.

32. M. A. Ali and P. Wahid, "Effect of Mutual Coupling in Adaptive Arrays," *Microwave and Optical Technology Letters*, **35**, 4, November 2002, pp. 270-274.

33. S. Werner, *Reduced Complexity Adaptive Filtering Algorithms with Applications to Communications Systems*, PhD dissertation, Helsinki University of Technology, Helsinki, Finland, October 2002.

34. G. D. Mandyam, N. Ahmed, and M. D. Srinath, "Adaptive Beamforming Based on the Conjugate Gradient Algorithm," *IEEE Transactions on Aerospace and Electronic Systems*, **33**, 1, January 1997, pp. 343-347.

35. Z. Rong, *Simulation of Adaptive Array Algorithms for CDMA Systems*, Master's thesis, Virginia Polytechnic Institute and State University, Blacksburg, VA, September 1996.

36. T. E. Biedka, J. H. Reed, and W. H. Tranter, "Mean Convergence Rate of a Decision Directed Adaptive Beamformer with Gaussian Interference," in IEEE Workshop on Sensor Array and Multichannel Signal Processing, March 2000, pp. 68-72.

37. S. Schell and W. Gardner, *Handbook of Statistics, Volume 10*, North-Holland, 1993, Chapter 18, pp. 755-817.

38.http://www.itl.nist.gov/div898/handbook/eda/section3/contour.htm